Journal of Systems Engineering and Electronics
Vol. 31, No. 4, August 2020, pp.692 – 702

Sensor scheduling for ground maneuvering target tracking in presence of detection blind zone

XU Gongguo[1,*], SHAN Ganlin[1], and DUAN Xiusheng[2]

1. Department of Electronic and Optical Engineering, Shijiazhuang Campus of Army Engineering University, Shijiazhuang 050003, China;
2. School of Mechanical Engineering, Shijiazhuang Tiedao University, Shijiazhuang 050013, China

Abstract: Continuous and stable tracking of the ground maneuvering target is a challenging problem due to the complex terrain and high clutter. A collaborative tracking method of the multi-sensor network is presented for the ground maneuvering target in the presence of the detection blind zone (DBZ). First, the sensor scheduling process is modeled within the partially observable Markov decision process (POMDP) framework. To evaluate the target tracking accuracy of the sensor, the Fisher information is applied to constructing the reward function. The key of the proposed scheduling method is forecasting and early decision-making. Thus, an approximate method based on unscented sampling is presented to estimate the target state and the multi-step scheduling reward over the prediction time horizon. Moreover, the problem is converted into a nonlinear optimization problem, and a fast search algorithm is given to solve the sensor scheduling scheme quickly. Simulation results demonstrate the proposed non-myopic scheduling method (Non-MSM) has a better target tracking accuracy compared with traditional methods.

Keywords: sensor scheduling, ground maneuvering target, detection blind zone (DBZ), decision tree optimization.

DOI: 10.23919/JSEE.2020.000044

1. Introduction

Tracking the ground target is much more difficult than the aerial target due to the complex terrain, high clutter, and strong target maneuvering. Therefore, the ground target detection sensors, such as ground moving target indicator (GMTI) and ground-based radar, mostly employ the pulse Doppler technology to eliminate the influence of ground clutters on the moving target indication [1 – 3], which has good detection performance for low-altitude targets [4]. However, this technology always set a detection threshold of minimum radial velocity of the target. It will cause a detection blind zone (DBZ) for the sensor when the target radial velocity is smaller than the detection threshold, which is called Doppler blindness [5,6]. Unlike the aerial target, the slower motion speed of the ground target make itself easy to become Doppler blindness for the detection sensor. Besides, the ground battlefield environment is more complex. The detection line of sight of the sensor may be occluded by mountains or tall buildings [7]. In this case, the target also cannot be detected by the detection sensor, which is called vision blindness. The above two kinds of DBZs can lead to the loss of target state, even track breakage and new track initiation. The quality of battlefield intelligence information will be seriously damaged.

Besides, different from traditional tracking scenes by a single sensor, multi-sensor collaborative working has been the development direction of military research [8]. As the main application, collaborative tracking by the multi-sensor network has received considerable attention from various aspects, which can effectively improve the tracking performance of the reconnaissance system [9,10]. However, for the complex problem of multi-sensor scheduling, the task requirements cannot be satisfied through manual decision-making. It is necessary and important to study the sensor management methods.

Up to now, the common sensor management methods include the covariance matrix based method [11,12], the information gain based method [13 – 15], and the operation risk based method [16 – 20]. For instance, Kalandros [11] proposed a multi-sensor selection method to improve the capability of the tracking platform, which selects sensor combinations based on the difference between the desired covariance matrix and the predicted covariance. Zhou et al. [12] proposed two control methods of the mobile sensor based on the trace and determinant of the covariance matrix. For wireless sensor network, Keshavarz et al. [13] proposed a sensor selection method based on the Fisher

Manuscript received May 14, 2019.
*Corresponding author.
This work was supported by the National Defense Pre-Research Foundation of China (0102015012600A2203).

information. Salvagnini et al. [14] studied the scheduling problem of camera sensors based on the information theory.

Recently, to improve the battlefield survivability of the radar network, Shi et al. [15,16] proposed two sensor scheduling methods with a low probability of interception. Moreover, a novel intercept probability factor was presented for multi-target tracking tasks in [17]. Zhang et al. [18,19] proposed a non-myopic sensor-scheduling method to select and assign active sensors for trading off the tracking accuracy and the radiation risk. Unlike Zhang, Marcos et al. [20] introduced a statistical risk based sensor management method in the target classification and tracking scenarios to reduce the potential operational risk.

However, most of the above sensor scheduling methods focus on the aerial target, while there are few research on the ground target considering the DBZ. In addition, the sensor model in the above research is simple, which always ignores the sensor dwell time. In order to maximize the tracking benefits, the switching frequency of the detection sensor is too fast, which is not in line with the actual situation and will consume more energy.

Based on the above analysis, to improve the tracking stability and tracking continuity of the ground maneuvering target in the complex environment, a non-myopic scheduling method (Non-MSM) of the multi-sensor system for the ground maneuvering target in the presence of DBZ is presented in this paper. Compared with the existing sensor scheduling methods, this method can be aware of DBZ in advance and maintain better target tracking performance of the ground maneuvering target all the time.

The rest of this paper is organized as follows. The scheduling problem is formulated within the partially observable Markov decision process (POMDP) framework in Section 2. The detailed scheduling process of the Non-MSM is presented in Section 3. Besides, the modified prediction method of the target state is given in Section 4. The scheduling problem is converted into an optimization problem in Section 5. Finally, simulation results are presented in Section 6, and conclusions are drawn in Section 7.

2. Problem formulation

POMDP is a mathematical model for decision analysis of the agent with partially observable and random environments. It has been successfully applied in many fields, such as path planning [21,22], system management [23–25], and text recognition [26,27]. Here, the POMDP model is suitable to deal with the scheduling problem because of the unobservable target state. The specific mathematical descriptions within the POMDP framework can be expressed as follows.

2.1 Scheduling action

Assuming that there are M sensors in the ground reconnaissance system, the scheduling action is denoted as $\boldsymbol{A}_k = [a_{1,k}, a_{2,k}, \ldots, a_{M,k}]$ at time step k, and $a_{m,k}$ $(1 \leqslant m \leqslant M)$ represents the action of the sensor m. Specifically, $a_{m,k} = 1$ represents that the sensor m works at time step k; otherwise, $a_{m,k} = 0$ represents that the sensor m does not work at time step k. Due to the limitation of energy and communication ability of the multi-sensor system, the number of the working sensors at the same time is limited. We define that the number of working sensors cannot exceed m_a, and there is

$$\sum_{m=1}^{M} a_{m,k} \leqslant m_a. \tag{1}$$

2.2 System state

The target motion process is described in the two-dimensional Cartesian coordinate system. Specially, the system state is denoted as $\boldsymbol{S}_k = \boldsymbol{X}_k$ at time step k, and $\boldsymbol{X}_k = [x_k, \dot{x}_k, y_k, \dot{y}_k]^{\mathrm{T}}$, where x_k and y_k are target position coordinates, $\dot{x}_k$ and $\dot{y}_k$ are target velocities. Because the real motion model of the maneuvering target is unknown, the target state transition law is given by

$$\boldsymbol{X}_{k+1} = \boldsymbol{F}_k^i \boldsymbol{X}_k + \boldsymbol{w}_k^i \tag{2}$$

where $\boldsymbol{F}_k^i$ is the state transition matrix which is selected from a mixed motion model set $\{\boldsymbol{F}_k^1, \boldsymbol{F}_k^2, \ldots, \boldsymbol{F}_k^\zeta\}$, ζ is the number of motion models; and $\boldsymbol{w}_k^i$ denotes the zero-mean white Gaussian process noise with the covariance matrix $\boldsymbol{Q}_k^i$ of the motion model $\boldsymbol{F}_k^i$. In general, two common models are employed, including the nearly constant velocity (NCV) model and the nearly constant turn (NCT) model. In the two-dimensional Cartesian coordinate system, the state transition matrices of the NCV model and the NCT model can be expressed as

$$\boldsymbol{F}_k^1 = \begin{bmatrix} 1 & \delta_t & 0 & 0 \\ 0 & 1 & 0 & 0 \\ 0 & 0 & 1 & \delta_t \\ 0 & 0 & 0 & 1 \end{bmatrix}, \tag{3}$$

$$\boldsymbol{F}_k^2 = \begin{bmatrix} 1 & \sin(\omega\delta_t)/\omega & 0 & -[1-\cos(\omega\delta_t)]/\omega \\ 0 & \cos(\omega\delta_t) & 0 & \sin(\omega\delta_t) \\ 0 & [1-\cos(\omega\delta_t)]/\omega & 1 & \sin(\omega\delta_t)/\omega \\ 0 & -\sin(\omega\delta_t) & 0 & \cos(\omega\delta_t) \end{bmatrix} \tag{4}$$

where δ_t is the sampling interval, and ω is the turn rate.

2.3 System measurement

The multi-sensor system measurement is denoted as $\boldsymbol{Z}_k = [(\boldsymbol{Z}_k^1)^{\mathrm{T}}, (\boldsymbol{Z}_k^2)^{\mathrm{T}}, \ldots, (\boldsymbol{Z}_k^m)^{\mathrm{T}}, \ldots, (\boldsymbol{Z}_k^M)^{\mathrm{T}}]^{\mathrm{T}}$ at time step k,

where $\boldsymbol{Z}_k^m$ denotes the measurement of sensor m. In general, the sensor measurement is obtained in the polar coordinate system with the sensor as the origin. Specially, the measurement value is composed of the target distance, azimuth and radial velocity, which can be written as

$$\boldsymbol{Z}_k^m = h_k^m(\boldsymbol{X}_k, a_{m,k}) + \boldsymbol{v}_k^m = [r_k^m, \theta_k^m, \dot{r}_k^m]^{\mathrm{T}} + \boldsymbol{v}_k^m \quad (5)$$

where $h_k^m(\cdot)$ is the measurement function of the sensor m, $\boldsymbol{v}_k^m$ denotes the zero-mean white Gaussian process noise of the sensor m with the covariance matrix $\boldsymbol{R}_k^m$, and r_k^m, θ_k^m and $\dot{r}_k^m$ are the distance, azimuth and radial velocity of the target, respectively, which can be calculated by

$$\begin{cases} r_k^m = \sqrt{(x_k - x_s^m)^2 + (y_k - y_s^m)^2} \\ \theta_k^m = \arctan \dfrac{y_k - y_s^m}{x_k - x_s^m} \\ \dot{r}_k^m = \dfrac{\dot{x}_k(x_k - x_s^m) + \dot{y}_k(y_k - y_s^m)}{\sqrt{(x_k - x_s^m)^2 + (y_k - y_s^m)^2}} \end{cases} \quad (6)$$

where x_s^m and y_s^m are the sensor position coordinates. Further, the system observation law can be expressed as

$$\boldsymbol{Z}_k = h_k(\boldsymbol{X}_k, \boldsymbol{A}_k) + \boldsymbol{V}_k = \begin{bmatrix} h_k^1(\boldsymbol{X}_k, a_{1,k}) \\ h_k^2(\boldsymbol{X}_k, a_{2,k}) \\ \vdots \\ h_k^M(\boldsymbol{X}_k, a_{m,k}) \end{bmatrix} + \begin{bmatrix} \boldsymbol{v}_k^1 \\ \boldsymbol{v}_k^2 \\ \vdots \\ \boldsymbol{v}_k^M \end{bmatrix} \quad (7)$$

where $h_k(\cdot)$ denotes the comprehensive measurement function of the multi-sensor system.

2.4 Reward based on Fisher information

To complete the POMDP model, we need a reward function to assess which sensor scheduling scheme can obtain a higher target tracking accuracy. Fortunately, the posterior Carmér-Rao lower bound (PCRLB) can reflect the sensor tracking performance, which can provide the lower bound of the target state estimation error in the future. According to [17], the PCRLB is the inverse of the Fisher information matrix. Moreover, Fisher information represents the amount of information obtained from the sensor measurement.

Thus, to avoid complex inversion calculations, we apply the Fisher information to assess the reward of the sensor scheduling action. Let $\boldsymbol{J}(\widehat{\boldsymbol{X}}_k)$ be the priori Fisher information matrix of the target at time step k and $\boldsymbol{J}(\widehat{\boldsymbol{X}}_{k+1}|\widehat{\boldsymbol{X}}_k, \boldsymbol{A}_{k+1})$ be the posterior Fisher information at time step $k+1$. When the target is detected by the sensor, the sensor measurement will be generated, and there is

$$\boldsymbol{J}(\widehat{\boldsymbol{X}}_{k+1}|\widehat{\boldsymbol{X}}_k, \boldsymbol{A}_{k+1}) = \boldsymbol{D}_k^{22} - \boldsymbol{D}_k^{21}[\boldsymbol{J}(\widehat{\boldsymbol{X}}_k) + \boldsymbol{D}_k^{11}]^{-1}\boldsymbol{D}_k^{12} + \boldsymbol{J}_{k+1}^{Z}(\boldsymbol{Z}_{k+1}) \quad (8)$$

with

$$\begin{cases} \boldsymbol{D}_k^{11} = \mathrm{E}[-\nabla_{\boldsymbol{X}_k}^{\boldsymbol{X}_k} \ln p(\widehat{\boldsymbol{X}}_{k+1}|\widehat{\boldsymbol{X}}_k)] \\ \boldsymbol{D}_k^{12} = [\boldsymbol{D}_k^{21}]^{\mathrm{T}} = \mathrm{E}[-\nabla_{\boldsymbol{X}_k}^{\boldsymbol{X}_{k+1}} \ln p(\widehat{\boldsymbol{X}}_{k+1}|\widehat{\boldsymbol{X}}_k)] \\ \boldsymbol{D}_k^{22} = \mathrm{E}[-\nabla_{\boldsymbol{X}_{k+1}}^{\boldsymbol{X}_{k+1}} \ln p(\widehat{\boldsymbol{X}}_{k+1}|\widehat{\boldsymbol{X}}_k)] \\ \boldsymbol{J}_{k+1}^{\boldsymbol{Z}} = \mathrm{E}[-\nabla_{\boldsymbol{X}_{k+1}}^{\boldsymbol{X}_{k+1}} \ln p(\boldsymbol{Z}_{k+1}|\widehat{\boldsymbol{X}}_{k+1})] \end{cases} \quad (9)$$

where the symbol ∇ represents the second-order derivative, the symbol E represents expectation, $\widehat{\boldsymbol{X}}_k$ is the estimated state at time step k, and $\boldsymbol{J}_{k+1}^{\boldsymbol{Z}}$ is the Fisher information gain from the sensor measurement $\boldsymbol{Z}_{k+1}$. When the target is occluded or the motion speed is too slow to be detected, the sensor measurement will not be generated, and the posterior Fisher information is only transferred from the prior information, and there is

$$\boldsymbol{J}(\widehat{\boldsymbol{X}}_{k+1}|\widehat{\boldsymbol{X}}_k, \boldsymbol{A}_{k+1}) = \boldsymbol{D}_k^{22} - \boldsymbol{D}_k^{21}[\boldsymbol{J}(\widehat{\boldsymbol{X}}_k) + \boldsymbol{D}_k^{11}]^{-1}\boldsymbol{D}_k^{12}. \quad (10)$$

$\boldsymbol{J}(\widehat{\boldsymbol{X}}_{k+1}|\boldsymbol{Z}_{k+1}, \boldsymbol{A}_{k+1})$ is a conditional entropy [28]. We can split the domain of integration for $p(\boldsymbol{Z}_{k+1}|\boldsymbol{A}_{k+1})$ into Ω^- and Ω^+, where Ω^- is the set in which the target cannot be detected and Ω^+ is the set in which the target can be detected. Further, (10) can be rewritten as

$$\begin{aligned} \boldsymbol{J}(\widehat{\boldsymbol{X}}_{k+1}|\widehat{\boldsymbol{X}}_k, \boldsymbol{A}_{k+1}) &= \int_{\Omega^+} p(\boldsymbol{Z}_{k+1}|\boldsymbol{A}_{k+1}) \int p(\widehat{\boldsymbol{X}}_{k+1}|\boldsymbol{Z}_{k+1}, \boldsymbol{A}_{k+1})\{\boldsymbol{D}_k^{22} - \boldsymbol{D}_k^{21}[\boldsymbol{J}(\widehat{\boldsymbol{X}}_k) + \boldsymbol{D}_k^{11}]^{-1}\boldsymbol{D}_k^{12} + \boldsymbol{J}_{k+1}^{Z}(\boldsymbol{Z}_{k+1})\} \cdot \\ & \mathrm{d}\widehat{\boldsymbol{X}}_{k+1}\mathrm{d}\boldsymbol{Z}_{k+1} + \int_{\Omega^-} p(\boldsymbol{Z}_{k+1}|\boldsymbol{A}_{k+1}) \int p(\widehat{\boldsymbol{X}}_{k+1}|\boldsymbol{Z}_{k+1}, \boldsymbol{A}_{k+1})\{\boldsymbol{D}_k^{22} - \boldsymbol{D}_k^{21}[\boldsymbol{J}(\widehat{\boldsymbol{X}}_k) + \boldsymbol{D}_k^{11}]^{-1}\boldsymbol{D}_k^{12}\}\mathrm{d}\widehat{\boldsymbol{X}}_{k+1}\mathrm{d}\boldsymbol{Z}_{k+1} = \\ & \int_{\Omega^+} p(\boldsymbol{Z}_{k+1}|\boldsymbol{A}_{k+1})\mathrm{d}\boldsymbol{Z}_{k+1}\boldsymbol{J}^+ + \int_{\Omega^-} p(\boldsymbol{Z}_{k+1}|\boldsymbol{A}_{k+1})\mathrm{d}\boldsymbol{Z}_{k+1}\boldsymbol{J}^- = \\ & \int_{\Omega^+} p(\boldsymbol{Z}_{k+1}|\boldsymbol{A}_{k+1})\mathrm{d}\boldsymbol{Z}_{k+1}\boldsymbol{J}^+ + [1 - \int_{\Omega^+} p(\boldsymbol{Z}_{k+1}|\boldsymbol{A}_{k+1})\mathrm{d}\boldsymbol{Z}_{k+1}]\boldsymbol{J}^- \end{aligned} \quad (11)$$

where $p(\boldsymbol{Z}_{k+1}|\boldsymbol{A}_{k+1})$ is the detection probability of the target; $\boldsymbol{J}^-$ and $\boldsymbol{J}^+$ are the Fisher information of Ω^- and Ω^+, respectively. Then, at time step k, we can use the following equation to calculate the optimal sensor scheduling action $\boldsymbol{A}_{k+1}^{\mathrm{opt}}$.

$$\boldsymbol{A}_{k+1}^{\mathrm{opt}} = \arg\max_{\boldsymbol{A}_{k+1}} \mathrm{trace}[\boldsymbol{J}(\widehat{\boldsymbol{X}}_{k+1}|\widehat{\boldsymbol{X}}_k, \boldsymbol{A}_{k+1})] = \arg\max_{\boldsymbol{A}_{k+1}} \mathrm{trace}\{\alpha_{k+1}(\boldsymbol{A}_{k+1})\boldsymbol{J}^+ + [1-\alpha_{k+1}(\boldsymbol{A}_{k+1})]\boldsymbol{J}^-\} \tag{12}$$

with

$$\alpha_{k+1}(\boldsymbol{A}_{k+1}) = \int_{\Omega^+} p(\boldsymbol{Z}_{k+1}|\boldsymbol{A}_{k+1})\mathrm{d}\boldsymbol{Z}_{k+1} \tag{13}$$

where $\alpha_{k+1}(\boldsymbol{A}_{k+1})$ is the weight of the Fisher information $\boldsymbol{J}^+$. Next, we study how to calculate the detection probability $p(\boldsymbol{Z}_{k+1}|\boldsymbol{A}_{k+1})$ for different situations.

To make the sensor scheduling model closer to the actual situation, the detection model is introduced to describe the complex environment. When considering the Doppler effect, the detection probability is related to the target radial velocity [29]. The detection probability $p(\boldsymbol{Z}_{k+1}|\boldsymbol{A}_{k+1})$ can be expressed as

$$p(\boldsymbol{Z}_{k+1}|\boldsymbol{A}_{k+1}) = \begin{cases} 0, & |\dot{r}_k^m| < V_{\min} \\ P_0\Big(1-\mathrm{e}^{-\ln 2(\frac{h(\dot{r}_k^m)}{V_{\min}})^2}\Big), & |\dot{r}_k^m| \geqslant V_{\min} \end{cases} \tag{14}$$

where $V_{\min}$ denotes the absolute value of the minimum radial velocity that can be detected by the sensor; $\dot{r}_k^m$ is the radial velocity of the target relative to the sensor; $h(\dot{r}_k^m)$ is the Doppler notch function. Assuming the target type is Swerling-I, the factor P_0 can be given by $P_0 = P_F^{1/(1+\mathrm{SNR})}$, where SNR is the signal to noise ratio, and P_F is the false alarm probability.

Moreover, the detection line of sight of the sensor may be occluded by obstacles sometimes. Let β_k be a binary variable which is used to indicate whether the target is occluded. Here, we adopt a simple model, and the detection probability $p(\boldsymbol{Z}_{k+1}|\beta_{k+1}, \boldsymbol{A}_{k+1})$ when considering the Doppler effect and obstacles is expressed as

$$p(\boldsymbol{Z}_{k+1}|\beta_{k+1}, \boldsymbol{A}_{k+1}) = \begin{cases} p(\boldsymbol{Z}_{k+1}|\boldsymbol{A}_{k+1}), & \beta_{k+1} = 0 \\ 0, & \beta_{k+1} = 1 \end{cases} \tag{15}$$

where $p(\boldsymbol{Z}_{k+1}|\boldsymbol{A}_{k+1})$ is calculated by (14).

3. Non-MSM

3.1 Definition

Traditional sensor scheduling methods mostly depend on the one-step prediction of the covariance matrix or information gain to determine the sensor scheduling action. However, one-step prediction cannot sense the changes of the target and the environment in time. In order to find the DBZ in advance and improve the target tracking accuracy, the Non-MSM is presented on the basis of the multi-step prediction strategy. In this method, the sensor scheduling action is determined not only based on the immediate reward but also the expected reward over a few time steps in the future. Compared with the sensor scheduling methods in [18], the goal of this paper is to improve the target tracking stability in the ground complex environment. The experiment conditions are more realistic, and the sensor cannot be switched at will.

Based on the above analysis, the reward function is denoted as $\boldsymbol{Q}$, and $\boldsymbol{Q}_h^\pi(\widehat{\boldsymbol{X}}_k)$ represents the total reward over h time steps, where $\widehat{\boldsymbol{X}}_k$ is the starting estimated state of the target. Then, we have

$$\boldsymbol{Q}_h^\pi(\widehat{\boldsymbol{X}}_k, h) = \mathrm{E}\left\{\sum_{\tau=0}^{h}\gamma^\tau \mathrm{trace}\left[\boldsymbol{J}(\widehat{\boldsymbol{X}}_{k+1+\tau}|\widehat{\boldsymbol{X}}_{k+\tau}, \boldsymbol{A}_{k+1+\tau})\right]\right\} = \underbrace{\mathrm{trace}\left[\boldsymbol{J}(\widehat{\boldsymbol{X}}_{k+1}|\widehat{\boldsymbol{X}}_k, \boldsymbol{A}_{k+1})\right]}_{\text{Immediate reward}} + \underbrace{\mathrm{E}\left\{\sum_{\tau=1}^{h}\gamma^\tau \mathrm{trace}\left[\boldsymbol{J}(\widehat{\boldsymbol{X}}_{k+1+\tau}|\widehat{\boldsymbol{X}}_{k+\tau}, \boldsymbol{A}_{k+1+\tau})\right]\right\}}_{\text{Future expected reward}} \tag{16}$$

where $\boldsymbol{A}_{k+1+\tau}$ is the scheduling action specified by the policy π at time step $k+1+\tau$, τ is the time variable, and γ is the discount factor [19].

Further, let $\boldsymbol{\pi}_h = [\boldsymbol{A}_{k+1}, \boldsymbol{A}_{k+2}, \ldots, \boldsymbol{A}_{k+1+h}]$ denote the sensor scheduling actions over h time steps in the future, then the sensor scheduling problem in this paper can be converted into the following nonlinear optimization problem.

$$\boldsymbol{\pi}_h^{\mathrm{opt}} = \arg\max_{\boldsymbol{A}_{k+1:k+1+h}} \boldsymbol{Q}_h^\pi(\widehat{\boldsymbol{X}}_k, h) = \arg\max_{\boldsymbol{A}_{k+1:k+1+h}} \left\{\mathrm{trace}[\boldsymbol{J}(\widehat{\boldsymbol{X}}_{k+1}|\widehat{\boldsymbol{X}}_k, \boldsymbol{A}_{k+1})] + \mathrm{E}\left\{\sum_{\tau=1}^{h}\gamma^\tau \mathrm{trace}[\boldsymbol{J}(\widehat{\boldsymbol{X}}_{k+1+\tau}|\widehat{\boldsymbol{X}}_{k+\tau}, \boldsymbol{A}_{k+1+\tau})]\right\}\right\} \tag{17}$$

where $\boldsymbol{\pi}_h^{\mathrm{opt}}$ represents the optimal sensor scheduling sequence over h time steps.

3.2 Non-myopic reward prediction

According to (17), we must know the future expected reward before calculating the non-myopic reward. However, the target state in the future cannot be known exactly. The common method is the Monte Carlo method which calculates the non-myopic reward through a lot of repeated experiments. However, it requires a large number of random samples regardless of the prediction time and the target number.

In view of the above problems, a non-myopic reward approximation method is proposed to reduce the computation complexity based on unscented sampling. This method will generate a certain number of particles according to the specific tracking scenario, which can reduce the computational complexity. The prediction method based on unscented sampling is shown in Fig. 1 and the specific steps can be briefly described as follows.

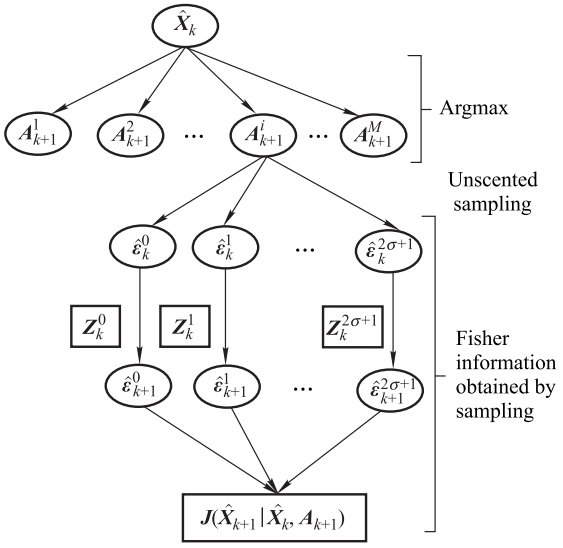

Fig. 1 Prediction method based on unscented sampling

Step 1 Assuming that the target estimation state and its covariance matrix are $\widehat{\boldsymbol{X}}_k$ and $\boldsymbol{P}_k$, then $2\sigma+1$ Sigma points ε^n_k and their weights β^n_k can be given according to (18) and (19).

$$\widehat{\varepsilon}^n_k = \begin{cases} \widehat{\boldsymbol{X}}_k, & n=0 \\ \widehat{\varepsilon}^0_k + [\sqrt{(\sigma+\lambda)\boldsymbol{P}_k}]_n, & n=1,2,\ldots,\sigma \\ \widehat{\varepsilon}^0_k - [\sqrt{(\sigma+\lambda)\boldsymbol{P}_k}]_n, & n=\sigma{+}1,\sigma{+}2,\ldots,2\sigma \end{cases} \tag{18}$$

$$\beta^n_k = \begin{cases} \dfrac{\lambda}{n+\lambda}, & n=0 \\ \dfrac{1}{2(n+\lambda)}, & n=1,2,\ldots,2\sigma \end{cases} \tag{19}$$

where σ is the dimension of ε^n_k, λ is the scale factor, and $[\ ]_n$ represents the nth line of the matrix after Cholesky decomposition of $\boldsymbol{P}_k$.

Step 2 On the basis of the Sigma points $\widehat{\varepsilon}^n_k$, transform the sampling points according to (20) and (21), and then get the measurements.

$$\widehat{\varepsilon}^n_{k+1|k} = \boldsymbol{F}^i_k \widehat{\varepsilon}^n_k + \boldsymbol{w}^i_k \tag{20}$$

$$\widehat{\boldsymbol{Z}}^n_{k+1} = h(\widehat{\varepsilon}^n_{k+1|k}) + \boldsymbol{v}_k \tag{21}$$

In order to estimate the future target state, it needs to know the target motion model. However, the real motion model of the maneuvering target is unknown. Fortunately, considering the motion continuity of the target, the motion model with the maximum distribution probability at the current time is adopted as the target motion model, that is

$$\boldsymbol{F}^i_k = \arg \max_{i=1,\ldots,\eta} \mu^i_k \tag{22}$$

where μ^i_k represents the distribution probability of motion model i.

Step 3 On the basis of $\widehat{\varepsilon}^n_{k+1|k}$ and $\widehat{\boldsymbol{Z}}^n_{k+1}$, update $\widehat{\varepsilon}^0_{k+1|k}, \widehat{\varepsilon}^1_{k+1|k}, \ldots, \widehat{\varepsilon}^{2\sigma}_{k+1|k}$ by the cubature Kalman filter (CKF) algorithm [30,31], and obtain the filter prediction states $\widehat{\varepsilon}^0_{k+1}, \widehat{\varepsilon}^1_{k+1}, \ldots, \widehat{\varepsilon}^{2\sigma}_{k+1}$. The future Fisher information by one-step prediction can be given by

$$\boldsymbol{J}(\widehat{\boldsymbol{X}}_{k+1}|\widehat{\boldsymbol{X}}_k, \boldsymbol{A}_{k+1}) = \sum_{n=1}^{2\sigma+1} [\beta^n_k \boldsymbol{J}(\widehat{\varepsilon}^n_{k+1}|\widehat{\boldsymbol{X}}_k, \boldsymbol{A}_{k+1})]. \tag{23}$$

Then, the future expected reward can be obtained by the multi-step iteration through (23).

4. Modified prediction of target state

In some special cases, the target will become the Doppler blindness for all sensors. It is impossible to update the target state by the CKF algorithm due to the lack of necessary measurements. The target state only can be obtained by prediction, the prediction method can be expressed as

$$\boldsymbol{X}_{k+1} = \boldsymbol{F}^i_k \boldsymbol{X}_k. \tag{24}$$

However, if the target is not detected because of the Doppler blindness. the motion state of the target is constrained, that is, the absolute value of the radial velocity of the target cannot be larger than the minimum radial velocity $V_{\min}$. It can be seen that the Doppler blindness itself is a kind of prior information. Based on the prior information, a modified prediction method of the target state is given.

Assuming that the target shown in Fig. 2 becomes the Doppler blindness for the sensor at time step $k+1$, it will not be observed at time $k+1$. The target state $\widehat{\boldsymbol{X}}_{k+1}$ at time step $k+1$ can only be got by the prediction method. For the target predicted state $\widehat{\boldsymbol{X}}_{k+1} = [\widehat{x}_{k+1}, \widehat{\dot{x}}_{k+1}, \widehat{y}_{k+1}, \widehat{\dot{y}}_{k+1}]^{\mathrm{T}}$, if the absolute value of the radial velocity relative to the sensor is still larger than the detection threshold $V_{\min}$, the predicted state needs to be modified. When $\widehat{\dot{r}}_{k+1} > V_{\min}$, the modified method is expressed as

$$\begin{cases} \widehat{\dot{x}}_{k+1} = \widehat{\dot{x}}_{k+1} - (\widehat{\dot{r}}_{k+1} - V_{\min}) \sin(\theta_{k+1}) \\ \widehat{\dot{y}}_{k+1} = \widehat{\dot{y}}_{k+1} - (\widehat{\dot{r}}_{k+1} - V_{\min}) \cos(\theta_{k+1}) \end{cases}. \tag{25}$$

When $\widehat{\dot{r}}_{k+1} < -V_{\min}$, the modified method is expressed

as

$$\begin{cases} \widehat{\hat{x}}_{k+1} = \widehat{\hat{x}}_{k+1} - (\widehat{\hat{r}}_{k+1} + V_{\min}) \sin(\theta_{k+1}) \\ \widehat{\hat{y}}_{k+1} = \widehat{\hat{y}}_{k+1} - (\widehat{\hat{r}}_{k+1} + V_{\min}) \cos(\theta_{k+1}) \end{cases} \tag{26}$$

where θ_{k+1} is the angle between the detection line of sight and the y direction, and $\widehat{\hat{r}}_{k+1}$ is the predicted radial velocity.

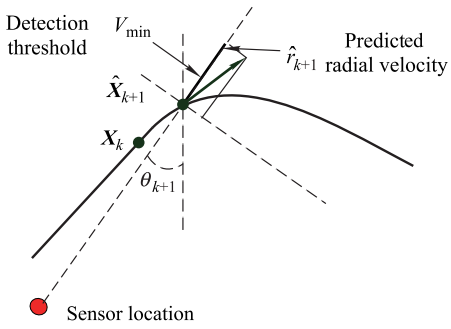

Fig. 2 Diagram of modified prediction method

5. Fast search algorithm (FSA)

It can be seen from (17) that the computation complexity of the optimization problem is very high, especially when the sensor number M and prediction horizon h are large. In addition, because the future target state is unknown, it may not be possible to calculate the optimal solution by the mathematical analytic method, and it is also difficult to match the real-time requirements of on-line scheduling. In the proposed Non-MSM, the prediction horizon h is finite. Thus, we can convert the sensor scheduling problem into a decision tree optimization problem.

Using the decision tree optimization algorithm, the filtering results of the previous nodes can be reused. Then, the repetitive complex filtering operation can be avoided, which can effectively accelerate the solving speed, especially for the large-scale sensor network. In this paper, we assume that one target only needs one sensor to track at each time. The depth and branch factors of the decision tree are equal to the length of the prediction time horizon and the number of sensors. In order to further improve the speed of the decision tree search algorithm, two pruning techniques are adopted to cut the branches of the decision tree during the search process.

(i) Pruning based on the sensor dwell time. When considering the sensor dwell time, it can be found that because the sensor has to work for a while before switching, the branches of the decision tree will be pruned a lot. When the sensor number is 2, the prediction time horizon h is 3, and the dwell time is 2, the decision trees with and without considering the sensor dwell time are shown in Fig. 3(a) and Fig. 3(b), respectively.

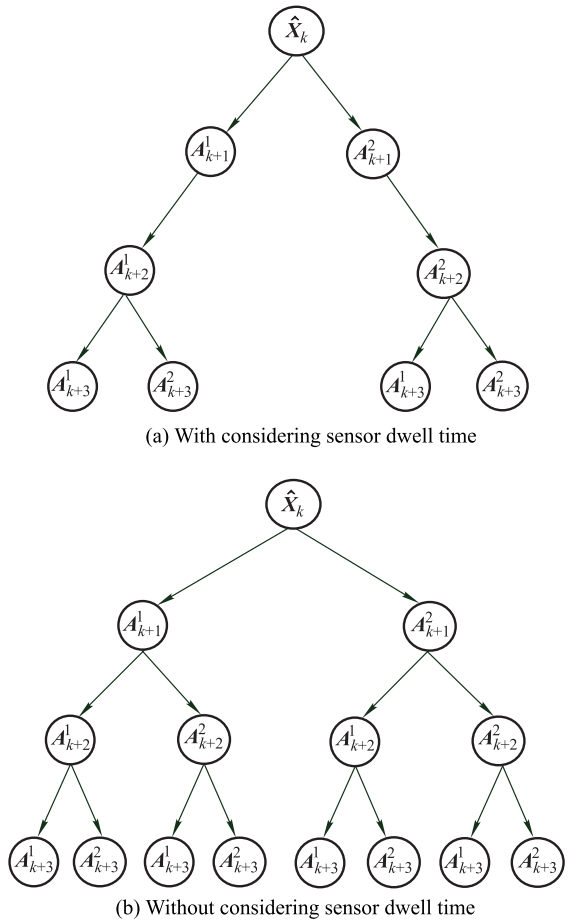

Fig. 3 Decision tree of sensor scheduling problem

(ii) Pruning based on the reward threshold. At first, the greedy search algorithm is used to find a global optimal solution quickly. The total reward value is defined as $R_{\max}$ and the cut-off factor is defined as η $(0 < \eta < 1)$. Then, if the cumulative reward value R_c of the current node satisfies (27) during searching, this node can be deleted, and the nodes after this node also do not need to open anymore.

$$R_c < \eta \frac{h_c R_{\max}}{h} \tag{27}$$

where h_c is the depth of the current node, h is the prediction time horizon, that is, the depth of the decision tree. This pruning strategy intuitively believes that a too small reward value at any depth cannot be a part of the optimal scheduling sequence with the maximum total reward. In summary, the proposed FSA for the sensor scheduling action based on the decision tree with pruning techniques can be described as Algorithm 1.

Algorithm 1 FSA

Step 1 Let $R_{\max} = 0$, and add the root node in the list.

Step 2 Use the greedy search algorithm to find an optimal solution $R_{\max}$, and execute Step 3.

Step 3 Remove the first node from the list, and open the children node of this node if it satisfies the sensor dwell time.

Step 4 If the depth h_c of the child node satisfies $h_c < h$ and the cumulative reward $R_c < \eta\dfrac{h_c R_{\max}}{h}$, cut the current child node.

If $h_c < h$ and $R_c \geqslant \eta\dfrac{h_c R_{\max}}{h}$, add the current child node in the list.

If $h_c = h$ and $R_c > R_{\max}$, choose R_c as $R_{\max}$.

Step 5 If the list is not empty, go to Step 2. Otherwise, terminate. Output the sensor scheduling sequence corresponding to the optimal solution $R_{\max}$.

Assuming that the computational complexity of each node in the decision tree is 1, when the sensor number is m and the prediction horizon is h ($h \geqslant 2$), the computational complexity is given by $O\left(\sum\limits_{i=1}^{h} m^h\right)$. Moreover, when the sensor dwell time is t ($2 \leqslant t \leqslant h$), the computational complexity is given by $O\left(\sum\limits_{i=1}^{h} m^h - \sum\limits_{j=1}^{t-1}\left[m^j \sum\limits_{i=1}^{h-j} m^i\right]\right)$.

Obviously, compared with the traditional search algorithm, the computational complexity of the proposed search algorithm will gradually decrease as the sensor dwell time and the prediction time horizon increase. Furthermore, the computational complexity will further decrease by the pruning technology based on the reward threshold.

6. Simulations

In this simulation, the effectiveness of the proposed Non-MSM for ground maneuvering target tracking is investigated. As shown in Fig. 4, four ground target detection sensors are used to track a maneuvering target. The deployment positions of the four sensors are (0.7, 3.5) km, (0.7, 1.0) km, (3.0, 0.5) km, and (3.0, 3.0) km. The sensor dwell time is 3 s and the detection threshold $V_{\min} = 5$ m/s. The standard deviations of range noise, azimuth noise, and radial velocity noise are 1.5 m, 0.01 rad, and 0.5 m/s, respectively. The power and energy of the sensor system are always limited. In order to avoid wasting resources, it is assumed that one target only needs one sensor to track each time.

Besides, there are four obstacles in the battlefield and the locations of the obstacles are shown in Fig. 4. The sampling interval $\delta_t = 1$ s and the simulation time is 100 s. The number of Monte Carlo experiments is 100. The initial position and velocity of the target are (0.5, 2.0) km and (30, 15) m/s, respectively. The target turns right during 25 – 40 s, turns left during 55 – 70 s, and maintains uniform motion during other time. The turn rate $\omega = 6$ rad/s. Three motion models are applied to the filter, which include the NCV model, the nearly left constant turn (NLCT) model and the nearly right constant turn (NRCT) model. The initial distribution probability of motion models is $\boldsymbol{\mu} = [0.34, 0.33, 0.33]$ and the transition probability matrix is

$$\boldsymbol{\Pi} = \begin{bmatrix} 0.90 & 0.05 & 0.05 \\ 0.05 & 0.90 & 0.05 \\ 0.05 & 0.05 & 0.90 \end{bmatrix}. \tag{28}$$

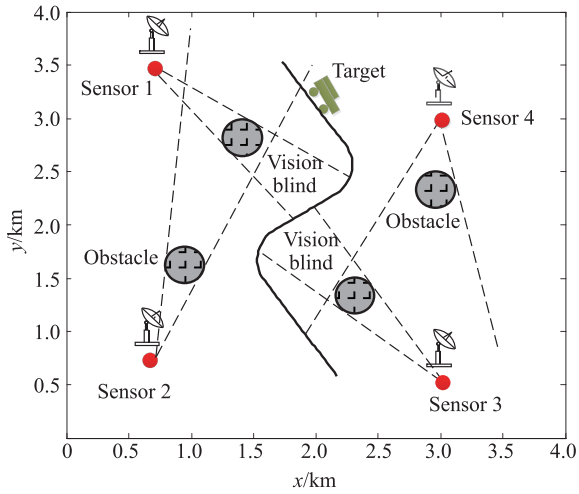

Fig. 4 Diagram of battlefield situation

The variation of the target radial velocity relative to different sensors is shown in Fig. 5. Obviously, for different sensors, there is time when the radial velocity is less than the detection threshold. In other words, the four sensors are unable to detect the target at some time. A single sensor cannot steadily track the target all the time. Thus, it is necessary to study the multi-sensor collaborative tracking method.

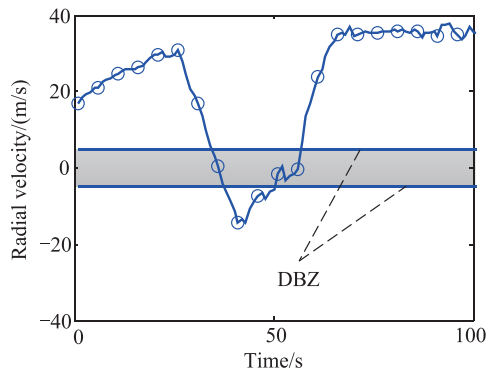

(a) Sensor 1

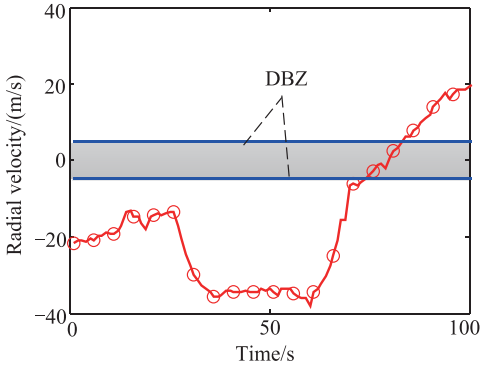

(b) Sensor 2

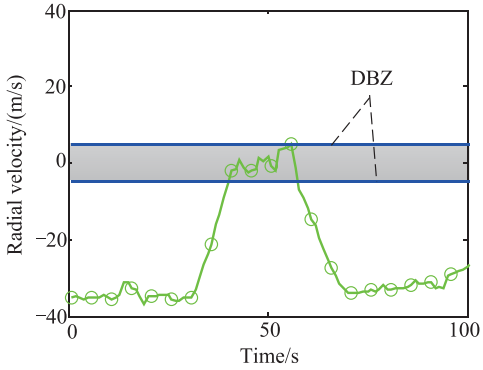

(c) Sensor 3

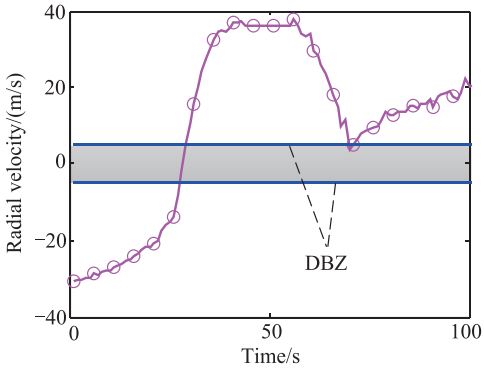

(d) Sensor 4

Fig. 5 Radial velocities of the target relative to different sensors

6.1 Comparison of scheduling methods

To clearly analyze the performance of the proposed Non-MSM, the fixed scheduling method (FSM), the nearest scheduling method (NSM), and the MSM [32,33] are used to do comparative experiments.

In the FSM, the sensor will not switch during the target tracking process. Sensor 2 is used to track the target all the time because the detection line of sight of sensor 2 is occluded less. In the NSM, the sensor which is closest to the target will be selected to track the target. In the MSM, sensor selection depends on the one-step prediction reward. Unlike MSM, sensor selection depends on the multi-step prediction reward in the proposed Non-MSM, and the prediction time horizon h is 3.

Fig. 6 shows the root mean square error (RMSE) of the target estimation position by different scheduling methods. It can be seen that the RMSE of the FSM will increase greatly at the beginning and around 80 s, and such great tracking error will result in loss of target track. Because of the obstacles and the Doppler blindness, Sensor 2 cannot detect the target at these times. Similarly, the RMSE of the NSM is still large at some time. The RMSE of the MSM is smaller than that of the FSM and the NSM. However, the myopic method selects the working sensor according to the one-step prediction reward, which cannot predict the DBZ in time. Therefore, the target tracking error of the MSM is larger than that of the Non-MSM at around 30 s and 75 s.

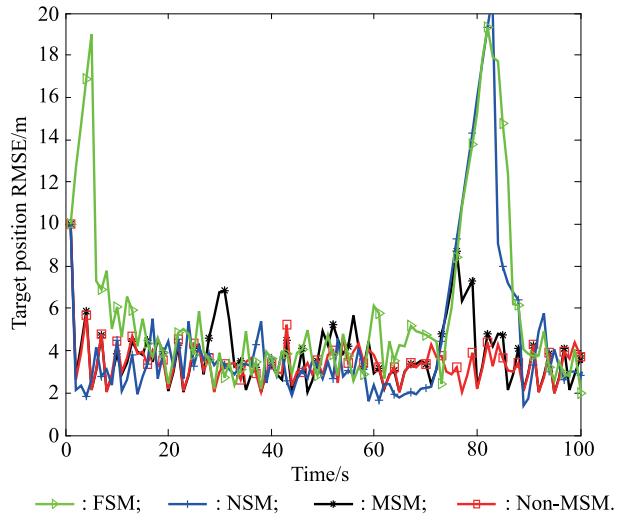

Fig. 6 RMSE of target estimation position

Compared with the other methods, we can clearly find that the RMSE of the target estimation position by Non-MSM is the smallest. The target tracking error is also stable and stays at a low level all the time. It is because that the proposed method can be aware of the DBZ in time. In this way, the most suitable sensor will be selected to track the target at each decision-making time.

The sensor scheduling schemes optimized by different methods are shown in Fig. 7. Compared with the MSM, the sensor switching frequency of the Non-MSM is less than that of the MSM. During the 100 Monte Carlo experiments, the number of sensor switching times of the Non-MSM is 21.52 on average, and the number of sensor switching times of the MSM is 24.37 on average. It is because of the farsightedness of the proposed method, which can save energy and extend the working life of the multi-sensor system.

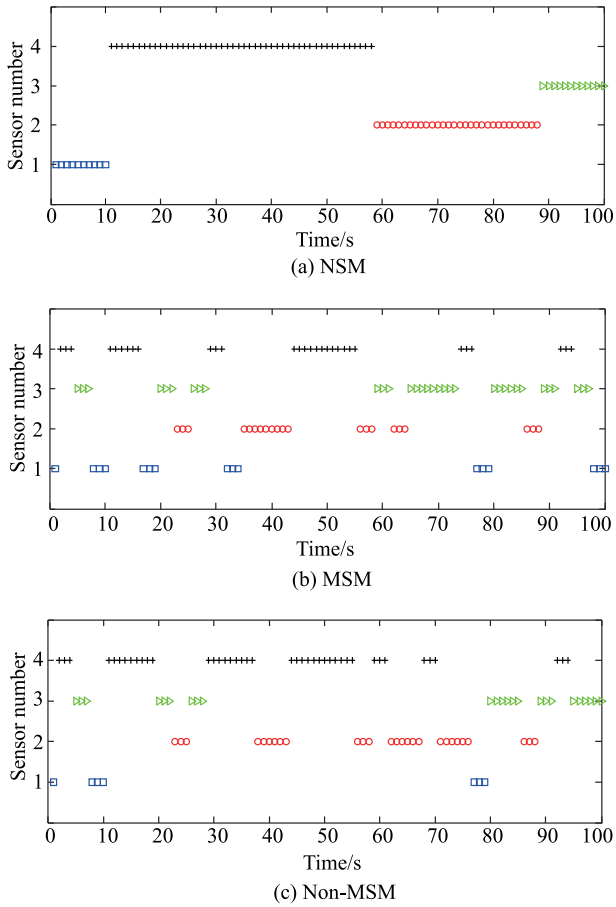

Fig. 7 Sensor selection schemes

It should be noted that h is the key parameter in the proposed sensor scheduling method. To analyze the influence of h on the target tracking accuracy, some experiments with different h are done to do comparison.

Fig. 8 shows the mean of RMSE versus prediction time horizon h. It can be seen that when $h \leqslant 4$, with the increasing h, the target tracking error will gradually decrease.

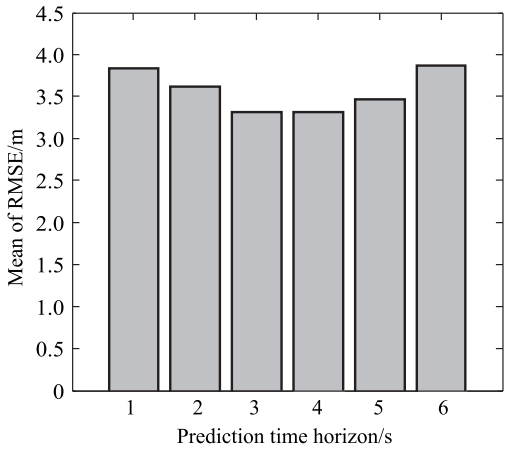

Fig. 8 The mean of RMSE

However, when $h > 5$, the tracking error increases with the increasing h. It is because the sensor scheduling scheme is determined by multi-step prediction. For the maneuvering target, as h increases, the prediction error of the system will also increase. The longer h is, the greater the prediction error is. Thus, when using the Non-MSM, the prediction time horizon should not be set too large. For the problem in this experiment, the best prediction time horizon is 3.

Meanwhile, to examine the effectiveness of the proposed FSA based on the decision tree optimization algorithm with pruning techniques, the depth-first search algorithm (DSA) is used to do comparison, and the average search time of a single decision is shown in Fig. 9. Obviously, the search time of the FSA is less than that of the DSA, and more running time will be saved with the increase of the prediction time horizon.

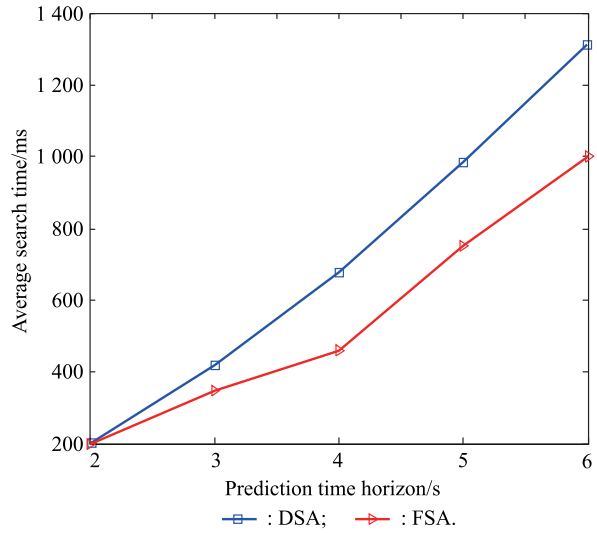

Fig. 9 Average search time of single decision

6.2 Comparison of target state prediction methods

To show the advantage of the proposed modified prediction method of the target state in the absence of measurements, the comparative experiment is carried out with the general prediction method. In the process of using the fixed sensor scheduling method, when the target becomes Doppler blindness for the detection sensor, the target state is predicted by two methods which include the modified prediction method and the general prediction method.

Fig. 10 shows the RMSE of the target prediction position by using the modified prediction method and the general prediction method. Compared with the general prediction method, we can see that the prediction error of the target state is reduced by the modified prediction method at around 80 s. Combined with Fig. 6, the target exactly be-

comes Doppler blindness for sensor 2 at around 80 s, which also corresponds to the variation of RMSE of the target estimation position. It can be concluded that the prediction error can be reduced by the modified prediction method. In this way, more accurate information can be provided for the subsequent track association operation, and the loss risk of the target track will be reduced.

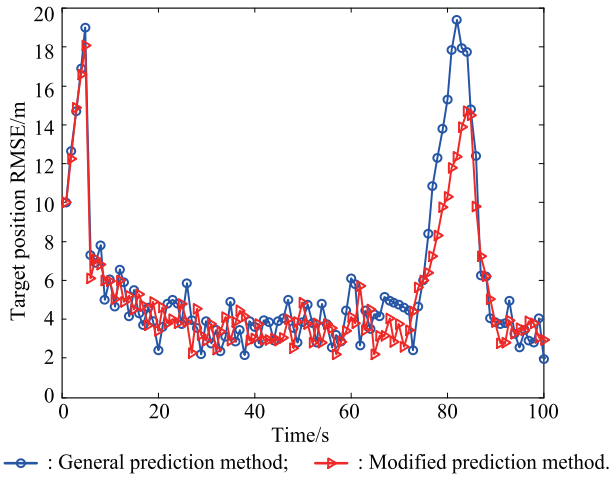

Fig. 10 RMSE of target prediction position by FSM

7. Conclusion and discussion

This paper presents a non-myopic multi-sensor collaborative scheduling method for tracking the ground maneuvering target in the presence of the DBZ. The method not only considers the immediate reward of the sensor scheduling action, but also takes into account the future expected reward over the prediction time horizon. Besides, an improved decision tree search algorithm based on the branch pruning techniques is proposed to solve the sensor scheduling action. Simulation results indicate that the method in this paper can select the most suitable sensor to track the target, and the target tracking accuracy is better than existing methods. The improved decision tree search algorithm can solve the scheduling scheme quickly, which also can be used to deal with other similar optimization problems.

However, only one target is considered in this paper, and the proposed method should be extended to the multi-target tracking case in future research.

References

[1] BUTT F A, JALIL M. An overview of electronic warfare in radar systems. Proc. of the International Conference on Technological Advances in Electrical, Electronics and Computer Engineering, 2013: 213 – 217.

[2] WAN K F, GAO X G, LI B, et al. Using approximate dynamic programming for multi-ESM scheduling to track ground moving targets. Journal of Systems Engineering and Electronics, 2018, 29(1): 74 – 85.

[3] HERNANDEZ M, BENAVOLI A, GRAZIANO A, et al. Performance measures and MHT for tracking move-stop-move targets with MTI sensors. IEEE Trans. on Aerospace and Electronic Systems, 2011, 47(2): 996 – 1025.

[4] MERTENS M, KIRUBARAJAN T, KOCH W. Doppler blind zone analysis for ground target tracking with bistatic airborne GMTI radar. Proc. of the IEEE 15th International Conference on Information Fusion, 2012: 2331 – 2338.

[5] MERTENS M, KOCH W, KIRUBARAJAN T. Exploiting Doppler blind zone information for ground moving target tracking with bistatic airborne radar. IEEE Trans. on Aerospace and Electronic Systems, 2014, 50(1): 130 – 148.

[6] HAN W, TANG Z Y, ZHU Z B. Method of target tracking with Doppler blind zone constraint. Journal of Systems Engineering and Electronics, 2013, 24(6): 889 – 898.

[7] JONGRAE K Y K. Moving ground target tracking in dense obstacle areas using UAVs. IFAC Proceedings Volumes, 2008, 41(2): 8552 – 8557.

[8] MODIEGINYANE K M, LETSWAMOTSE B B, MALEKIAN R, et al. Software defined wireless sensor networks application opportunities for efficient network management: a survey. Computers & Electrical Engineering, 2018, 66(3): 274 – 287.

[9] ANGLEY D, RISTIC B, SUVOROVA S, et al. Non-myopic sensor scheduling for multistatic sonobuoy fields. IET Radar, Sonar and Navigation, 2017, 11(12): 1770 – 1775.

[10] NAYEBI A A, PARIZ N, NAGHIBI S M. Adaptive node scheduling under accuracy constraint for wireless sensor nodes with multiple bearings-only sensing units. IEEE Trans. on Aerospace and Electronic Systems, 2015, 51(2): 1547 – 1557.

[11] KALANDROS M. Covariance control for multisensor systems. IEEE Trans. on Aerospace and Electronic Systems, 2002, 38(4): 1138 – 1157.

[12] ZHOU K, ROUMELIOTIS S. Optimal motion strategies for range-only constrained multisensor target tracking. IEEE Trans. on Robotics, 2008, 24(5): 1168 – 1185.

[13] KESHAVARZ-M A, KHALOOZADEH H. Interacting multiple model and sensor selection algorithms for manoeuvering target tracking in wireless sensor networks with multiplicative noise. International Journal of Systems Science, 2017, 48(5): 899 – 908.

[14] SALVAGNINI P, PERNICI F, CRISTANI M, et al. Non-myopic information theoretic sensor management of a single pan-tilt-zoom camera for multiple object detection and tracking. Computer Vision and Image Understanding, 2015, 134(5): 74 – 88.

[15] SHI C G, WANG F, SALOUS S, et al. Joint transmitter selection and resource management strategy based on low probability of intercept optimization for distributed radar networks. Radio Science, 2018, 53(9): 1108 – 1134.

[16] SHI C G, ZHOU J J, WANG F. LPI based resource management for target tracking in distributed radar network. Proc. of the IEEE Radar Conference, 2016: 822 – 826.

[17] XU G G, PANG C, DUAN X S, et al. Multi-sensor optimization scheduling for target tracking based on PCRLB and a novel intercept probability factor. Electronics, 2019, 8(2): 140 – 162.

[18] ZHANG Z Z, SHAN G G. Non-myopic sensor scheduling to track multiple reactive targets. IET Signal Processing, 2015, 9(1): 37 – 47.

[19] ZHANG Z Z, SHAN G G. UTS-based foresight optimization of sensor scheduling for low interception risk tracking. International Journal of Adaptive Control and Signal Processing, 2014, 28(10): 921 – 931.

[20] MARCOS E G, DOMINIQUE M, PHILIPPE V, et al. A

risk-based sensor management using random finite sets and POMDP. Proc. of the IEEE 20th International Conference on Information Fusion, 2017: 1 – 9.
[21] SHANKARACHARY R, CHONGE K P. UAV path planning in a dynamic environment via partially observable Markov decision process. IEEE Trans. on Aerospace and Electronic Systems, 2013, 49(4): 2397 – 2412.
[22] EATON C M, CHONGE K P, MACIEJEWSKI A A. Robust UAV path planning using POMDP with limited FOV sensor. Proc. of the IEEE Conference on Control Technology and Applications, 2017: 1530 – 1535.
[23] MYERS V, WILLIAMS D P. A POMDP for mulit-view classification with an autonomous underwater vehicle. Proc. of the IEEE Conference on Oceans, 2010. DOI: 10.1109/OCEANS.2010.5664609.
[24] WILLIAMS B K. Resolving structural uncertainty in natural resources management using POMDP approaches. Ecological Modeling, 2011, 222(5): 1092 – 1102.
[25] YOUNG S, GASIC M, KEIZER S, et al. The hidden information state model: a practical framework for POMDP-based spoken dialogue management. Computer Speech and Language, 2010, 24(2): 150 – 174.
[26] WANG Z R, DU J, WANG W C, et al. A comprehensive study of hybrid neural network hidden Markov model for offline handwritten Chinese text recognition. International Journal on Document Analysis and Recognition, 2018, 21(2): 1 – 11.
[27] AISWARYA V, RAJU N N, JOY S S J, et al. Hidden Markov model-based sign language to speech conversion system in TAMIL. Proc. of the IEEE 4th International Conference on Biosignals, Images and Instrumentation, 2018: 206 – 212.
[28] DENZLER J, BROWN C M. Information theoretic sensor data selection for active object recognition and state estimation. IEEE Trans. on Pattern Analysis & Machine Intelligence, 2002, 24(2): 145 – 157.
[29] MERTENS M, NICKEL U. GMTI tracking in the presence of Doppler and range ambiguities. Proc. of the 14th International Conference on Information Fusion, 2011: 1 – 8.
[30] ARASARATNAM I, HAYKIN S. Cubature Kalman filters. IEEE Trans. on Automatic Control, 2009, 54(6): 1254 – 1269.
[31] ARASARATNAM I, HAYKIN S, HURD T R. Cubature Kalman filtering for continuous-discrete systems: theory and simulations. IEEE Trans. on Signal Processing, 2013, 58(10): 4977 – 4993.
[32] SAYARSHAD H R, GAO H O. A non-myopic dynamic inventory routing and pricing problem. Transportation Research Part E: Logistics and Transportation Review, 2018, 109(1): 83 – 98.
[33] SONG H, XIAO M, XIAO J, et al. A POMDP approach for scheduling the usage of airborne electronic countermeasures in air operations. Aerospace Science and Technology, 2016, 48(1): 86 – 93.

Biographies

XU Gongguo was born in 1990. He received his B.S. degree from University of Science and Technology of China in 2014, and M.S. degree from Army Engineering University in 2017. Now, he is a Ph.D. candidate in Army Engineering University. His research interests include multi-sensor management and information fusion.
E-mail: xugguo@yeah.net

SHAN Ganlin was born in 1962. He received his B.S., M.S. and Ph.D. degrees from Nanjing University of Science and Technology in 1983, 1991 and 1994, respectively. Now, he is a professor at Army Engineering University. His research interests include air defense weapon system and information fusion.
E-mail: shanganlin@163.com

DUAN Xiusheng was born in 1970. He received his B.S. and M.S. degrees from College of Electronic Engineering in 1993 and 1996, and Ph.D. degree from Army Engineering University in 2009. Now, he is a professor at Shijiazhuang Tiedao University. His research interests include failure diagnosis and information fusion.
E-mail: sjzdxsh@163.com